Nuclear Materials and Energy 42 (2025) 101853

Contents lists available at ScienceDirect

Nuclear Materials and Energy

journal homepage: www.elsevier.com/locate/nme

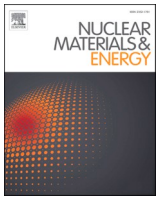

Study of the $^{2}H(^{3}He, p_0)^{4}He$ nuclear reaction for deuterium depth profiling

Varvara Foteinou [a,*], Fotios Maragkos [a,b], Hans-Werner Becker [a], Michael Kokkoris [b], Matej Mayer [c], Georgios Provatas [d], Detlef Rogalla [a], Thomas Schwarz-Selinger [c]

[a] Central Unit for Ion Beams and Radionuclides, Ruhr University Bochum, 44801 Bochum, Germany
[b] Department of Physics, National Technical University of Athens, 15780 Athens, Greece
[c] Max Planck Institute for Plasma Physics, 85748 Garching, Germany
[d] Division of Experimental Physics, Ruđer Bošković Institute, 10000 Zagreb, Croatia

ARTICLE INFO

Keywords:
Deuterium profiling
Nuclear reaction analysis
Fusion materials

ABSTRACT

The differential cross sections of the $^{2}H(^{3}He, p_0)^{4}He$ reaction have been determined at six detection angles (120°, 130°, 140°, 150°, 160° and 170°) in the energy range between 300 and 4000 keV, with steps of 30 to 100 keV. The measurements were performed at the 4 MV Dynamitron Tandem Laboratory of the Central Unit for Ion Beams and Radionuclides of the Ruhr University Bochum in Germany. A thin layer of amorphous deuterated hydrocarbon (a-C:D) plasma-deposited on a chromium substrate was used in all measurements. Overall, the results of the present study are in very good agreement with differential cross-section data available in the literature for similar detection angles, with an average deviation of less than 6 %.

1. Introduction

Deuterium, one of the two stable isotopes of hydrogen, is in comparison to protium notable for its higher melting point, higher boiling point and higher critical temperature and pressure. In addition, the chemical bonds involving deuterium are rather stronger than the equivalent bonds in protium. These properties, combined with the fact that it is hardly hazardous to health, have resulted in deuterium being used in various fields, such as in medicinal chemistry, semiconductors, biotechnology and, of course, in fusion research, where, mainly due to the energy release in fusion reactions, deuterium is utilized as fuel in controlled fusion devices such as the JET and the ITER tokamaks [1,2]. Thus, the accurate quantitative determination and depth profiling of deuterium is essential, particularly for fusion, where assessing the deposition of deuterium on the materials exposed to the fusion plasma is of utmost importance [2,3].

Nuclear Reaction Analysis (NRA), and specifically the $^{2}H(^{3}He, p_0)^{4}He$ reaction, has been found to be optimal for the quantification and depth profiling of deuterium at depths of up to a few tens of μm [3] and is therefore regularly employed for deuterium analysis. Nevertheless, for energies in the MeV range, often implemented for NRA applications, the differential cross section of this reaction has, so far, been measured at only three backward detection angles, namely 135°, 144.5° and 175° [4–6]. These datasets, though, are quite regularly used also for different detection angles. At low energies, this approach introduces minimal errors since the cross section of this reaction is nearly angle-independent in the center-of-mass system at beam energies below approximately 1200 keV [7–10]. However, at higher energies — where many applications are performed for studying larger depths — this approach may, of course, lead to systematic errors. The aim of this work was to systematically study the differential cross sections of the $^{2}H(^{3}He, p_0)^{4}He$ reaction over a range of angles and energies relevant to NRA applications (namely $\theta = 120° - 170°$, $E_{lab} = 300 - 4000$ keV), to assess the angular dependence at higher energies, and to contribute coherent differential cross-section data to the existing literature.

2. Experimental setup

The measurements were performed at the Dynamitron Tandem Laboratory of the Central Unit for Ion Beams and Radionuclides (RUBION) of the Ruhr University Bochum in Germany. The experimental setup consisted of a high-precision goniometer (0.1°), onto which six silicon surface barrier (SSB) detectors of 1500 μm in thickness were placed at 120°, 130°, 140°, 150°, 160° and 170°, with respect to the beam direction. The distance between the detectors and the target was approximately 7.5 cm. To reduce the azimuthal angular uncertainty (<±1.5°), orthogonal tantalum slits (~4×8 mm^2) were placed in front of the detectors. In addition, cylindrical aluminum tubes of 3.4 cm in

* Corresponding author.
E-mail address: Varvara.Foteinou@rub.de (V. Foteinou).

https://doi.org/10.1016/j.nme.2024.101853
Received 28 October 2024; Received in revised form 8 December 2024; Accepted 19 December 2024
Available online 20 December 2024

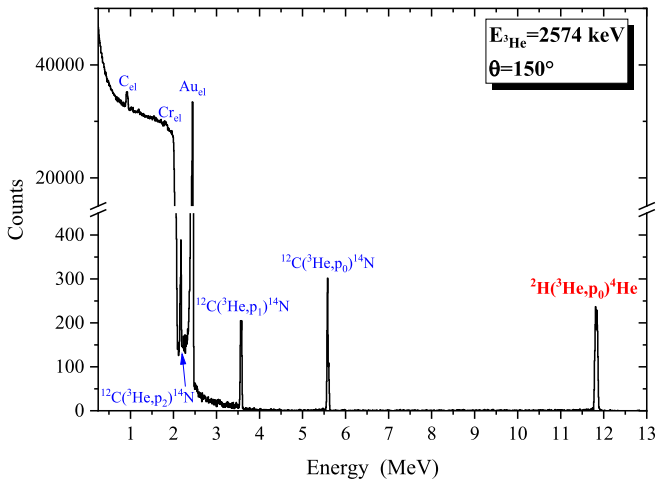

Fig. 1. Typical experimental spectrum collected at E_{lab} = 2574 keV and θ = 150°.

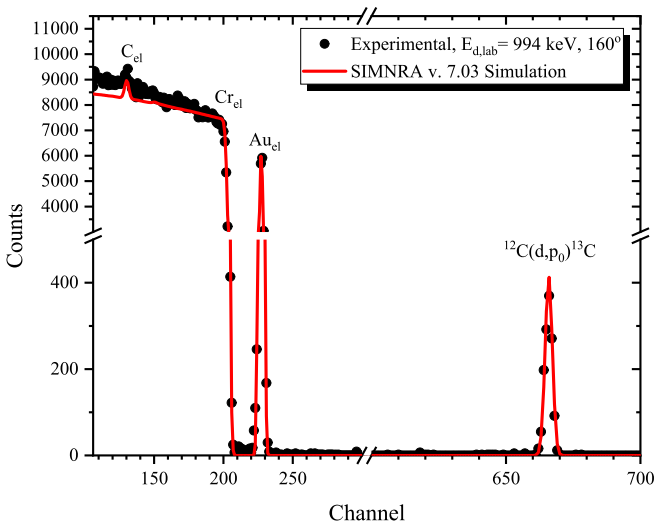

Fig. 2. Analysis of the target used in the differential cross-section measurements with a deuteron beam of 994 keV at θ = 160°.

length and in 1.1 cm inner diameter were placed in front of the detectors to reduce the background arising by scattering on the chamber walls and the Faraday cup. The entire setup was housed in a cylindrical scattering chamber with a diameter of ~50 cm. Further details about the experimental setup can be found in [11].

The ^{3}He beam was provided by the 4 MV Tandem Dynamitron accelerator at energies between 300 and 4000 keV, in steps of 30 to 100 keV. The diameter of the beam spot was ~3 mm, while the current ranged between 15 and 50 nA. The magnetic constant of the analyzer magnet was determined by the measurement of the 992-keV resonance of the ^{27}Al(p, γ)^{28}Si reaction. This measurement confirmed previous systematic studies performed at the RUBION laboratory for the determination of the magnetic constant [12].

All measurements were performed using the same target, which consisted of a thin layer (~100 nm) of amorphous deuterated hydrocarbon (a-C:D) grown by plasma deposition on a bulk chromium substrate (~400 μm). The target was manufactured at the Max Planck Institute for Plasma Physics in Garching, Germany. Details about the manufacturing process can be found in [13]. For current normalization and to ensure thermal stability, an ultra-thin Au film (~5 nm) was evaporated onto its surface in RUBION. A typical spectrum collected at E_{lab} = 2574 keV and θ = 150° is presented in Fig. 1, where the peaks labeled as "el" correspond to elastic scattering.

3. Data analysis

With the aim of minimizing the uncertainties in the reported differential cross-section values and, in particular, to avoid errors in the measurement of the beam current and the solid angles covered by the detectors, the cross sections were determined relative to the elastic scattering on Au by the following expression:

$$\left(\frac{d\sigma}{d\Omega}\right)^{D}_{E,\theta} = \left(\frac{d\sigma}{d\Omega}\right)^{Au,Ruth}_{E',\theta} \times \frac{Y_D}{Y_{Au}} \times \frac{N_{Au}}{N_D} \quad (1)$$

where E and E' correspond to the beam energies in the center of the CD and Au layer, respectively, θ is the detection angle, Y_D is the integrated area of the ^{2}H(^{3}He, p$_0$)^{4}He peak, Y_{Au} the integrated area of the Au elastic peak, N_{Au} and N_D are respectively the atomic areal densities of Au and D in the target and $\left(\frac{d\sigma}{d\Omega}\right)^{Au,Ruth}_{E',\theta}$ is the screening-corrected Rutherford differential cross section for the elastic scattering of ^{3}He on Au at beam energy E' and detection angle θ.

The effective beam energies E and E' were calculated with the SIMNRA v. 7.03 code [14] utilizing the SRIM2013 [15] stopping power data. The Y_D and Y_{Au} peak areas were determined using the TV code, a Fortran-based spectral analysis program for UNIX systems, specifically designed for peak integration and fitting. Further details about the TV code can be found in [16]. It is important to point out that the ^{2}H(^{3}He, p$_0$)^{4}He peak was isolated and nearly background-free in all spectra, resulting in statistical uncertainties in Y_D of less than 5 %. The corresponding uncertainties in the integration of the Au elastic peak were below 0.6 %.

The areal density of D in the target (N_D) was calculated from the areal density of ^{12}C by assuming that the D/(C+D) ratio is equal to 0.34, same as for C:H films prepared previously under similar conditions [17]. For the determination of the ^{12}C and ^{197}Au areal densities, the NRA and RBS techniques were respectively applied by using a deuteron beam at E_d = 994 keV. The experimental spectrum collected at the detection angle θ = 160°, is presented in Fig. 2 together with simulation performed by the SIMNRA v. 7.03 code. For the simulation, the SRIM2013 stopping power data and the straggling model of Chu and Yang [18] were employed, together with evaluated differential cross sections for the ^{12}C(d, p$_0$)^{13}C reaction [19] and the Rutherford differential cross sections for the elastic scattering on ^{197}Au. According to this analysis, the atomic areal densities of D and Au are equal to (368 ± 26)•10^{15} at/cm^2 and (34.4 ± 2.4)•10^{15} at/cm^2, respectively, resulting in a value of 0.0935 ± 0.0018 for the N_{Au}/N_D ratio. The uncertainties reported for the absolute values of the D and Au areal densities include the errors in the measurement of the beam current and solid angle as well as the statistical errors from the integration of the experimental peaks, while the uncertainty for the N_{Au}/N_D ratio includes only the statistical errors from the integration of the corresponding peaks. Finally, to investigate the lateral homogeneity of the target, the target was irradiated with a 994-keV deuteron beam at 3 different positions. The differences in the yields of the Au and C peaks were found to be lower than 2.3 %.

The most critical part of this work was to accurately quantify the deuterium loss from the target during the measurements. For this purpose, in the same experiment, 12 additional measurements were conducted at previously measured energies. These measurements were taken at regular intervals during the experiment (every ~300 keV). Provided that the deuterium loss is proportional to the beam charge accumulated on the target during each measurement, a correction factor, f, was calculated according to:

$$f = a \cdot \Sigma Q + \beta \quad (2)$$

For each measurement, the beam charge Q was determined from the elastic peak of ^{197}Au in the experimental spectrum and the

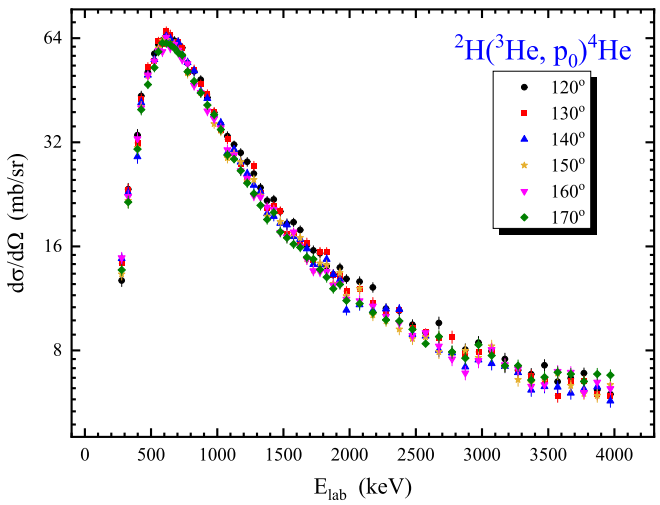

Fig. 3. Energy and angular variation of the differential cross-section values obtained in the current work for the ^{2}H(^{3}He, p$_0$)^{4}He reaction. The error bars include the statistical uncertainties from the determination of the peak areas as well as uncertainties on the correction factor applied for deuterium loss.

corresponding Rutherford cross-section value. The total charge, ΣQ, for each measurement, was calculated by summing the charge, Q, of the current measurement with the accumulated charge from all previous ones. To determine the parameters α and β, all 12 additional measurements at the 6 detection angles were utilized, resulting in a total of 72 spectra. Specifically, for each repeated measurement, a correction factor, f, was determined based on the differences in the yield of the ^{2}H(^{3}He, p$_0$)^{4}He reaction peak. The α and β parameters were then derived through linear fitting of all 72 available values. The uncertainties of α and β, obtained from the fitting process, were used to estimate the uncertainty of the correction factor f, which was found to be less than 1 %. The evaluation described above confirmed that deuterium loss is proportional to the beam charge accumulated on the target and remains independent of the beam current within the range used in this experiment (15–50 nA). The total deuterium loss throughout the experiment amounted to approximately 13 %.

4. Results and discussion

The differential cross-section values derived from this work for the ^{2}H(^{3}He, p$_0$)^{4}He reaction ranged from 5.7 to 67.3 mb/sr with a total estimated uncertainty between 3.7 % and 5.5 %. The errors contributing to the total estimated uncertainty are listed in Table 1 in the appendix. In accordance with the instructions given in [20], the total estimated uncertainty includes statistical errors from the integration of the ^{2}H(^{3}He,

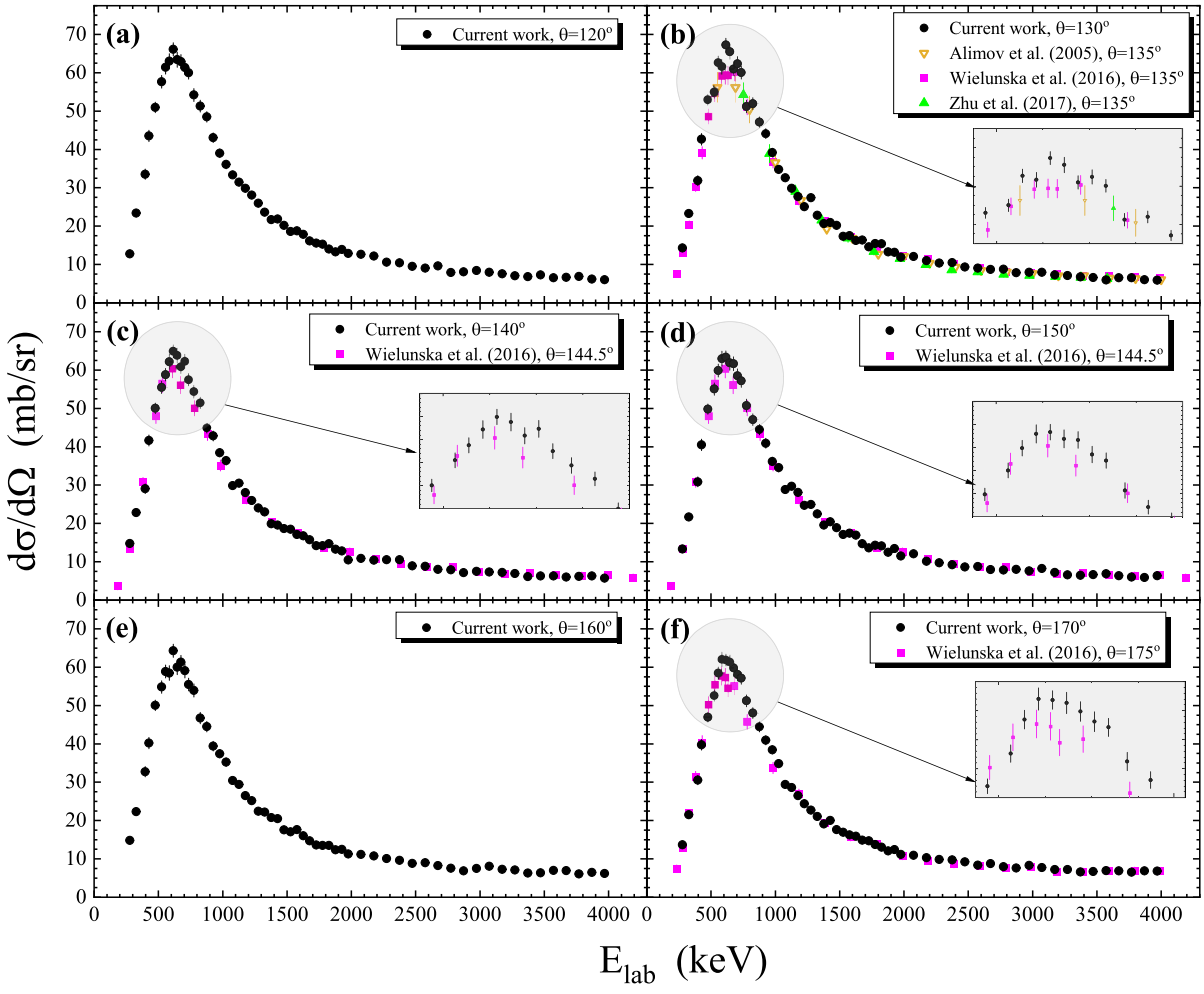

Fig. 4. Differential cross sections of the ^{2}H(^{3}He, p$_0$)^{4}He reaction determined at the scattering angles of (a) 120°, (b) 130°, (c) 140°, (d) 150°, (e) 160° and (f) 170°. The data determined in the present work are presented with black dots. The solid squares correspond to the data of Wielunska et al. [5] at 135°, 144.5° and 175°, while the solid and open triangles correspond respectively to the data of Zhu et al. [6] and Alimov et al. [4] at 135°. The error bars include the statistical uncertainties resulting from the determination of the peak areas as well as uncertainties on the correction factor applied for the deuterium loss.

$p_0)^4$He reaction peak (2.0–4.6 %) and the Au scattering peak (<0.6 %) as well as the uncertainties resulting from the determination of the N_{Au}/N_D ratio (1.9 %), the inhomogeneity of the target (2.3 %) and the correction factor applied for the deuterium loss (<1 %). The uncertainty in the beam energy was ~2 keV, which resulted from the energy ripple of the accelerator (0.4 keV), the uncertainty in the magnetic constant (0.07 %) [12] and the beam straggling inside the target, as calculated using the SIMNRA code.

The differential cross sections determined in the present work are given in Table 2 in the appendix and are also presented in Fig. 3. The cross-section errors included in Table 2 correspond to the total estimated uncertainties, whereas the error bars in Fig. 3 represent only the statistical uncertainties from the determination of the peak areas and those arising from the deuterium-loss correction factor. As shown in Fig. 3, while the cross section is indeed nearly angle-independent at low beam energies, this clearly does not hold for energies above approximately 1200 keV, as the differences between the values for the various detection angles can reach up to 16 %, even when accounting for statistical errors.

The results of this work are also presented in Fig. 4 together with data available in literature for detection angles close to the ones investigated here. Notably, the only available datasets in the literature suitable for NRA applications in the MeV energy range, are those by Wielunska et al. [5] at 135°, 144.5° and 175° (solid squares in Fig. 4b,c, d,f) and the ones by Alimov et al. [4] and Zhu et al. [6] at 135° (open and solid triangles in Fig. 4b). Apart from the maxima of the resonance at ~630 keV, all datasets are overall in almost excellent agreement with the present values. However, the maxima of the resonance seem to be underestimated, while in Fig. 4c and 4f there is also an indication that the width of the resonance is smaller compared to the present data. Nevertheless, this does not apply to the comparisons shown in Fig. 4b and 4d, making it impossible to derive any definitive conclusions. It should be noted that for low energies, in addition to the literature data presented in Fig. 4, differential cross sections can be derived from total cross-section measurements available in the literature by assuming angular independence in the center-of-mass system. Moreover, there is also literature available regarding the inverse reaction ^{3}He(^{2}H, $p_0)^4$He. Details concerning the two latter cases can be found in [7,8,21].

5. Summary and conclusions

The differential cross sections of the ^{2}H(^{3}He, $p_0)^4$He reaction have been determined at six backward angles ranging from 120° to 170°, with a step of 10°, and at energies between 300 and 4000 keV, in steps of 30 to 100 keV. All measurements were performed at the RUBION facility of the Ruhr University Bochum in Germany. The target used in the measurements consisted of three layers, an ultra-thin Au layer, a thin amorphous deuterated hydrocarbon (a-C:D) layer and a chromium substrate. The determined cross-section values ranged between 5.7 and 67.3 mb/sr with a total estimated uncertainty that did not exceed 5.5 %. The cross section is dominated by a broad resonance at around 630 keV and is particularly flattened at higher energies. This fact, in combination with the high-energy and almost background-free reaction peak, renders this reaction very well suited for NRA applications. However, an angular dependence of the cross-section values was observed for energies exceeding approximately 1200 keV, indicating that the positioning of the detectors should also be considered. All data obtained in this work will soon be available at the IBANDL website (https://www-nds.iaea.org/exfor/ibandl.htm).

CRediT authorship contribution statement

Varvara Foteinou: Writing – original draft, Validation, Supervision, Resources, Project administration, Methodology, Investigation, Funding acquisition, Formal analysis, Data curation, Conceptualization, Visualization. **Fotios Maragkos:** Writing – review & editing, Investigation, Formal analysis, Conceptualization. **Hans-Werner Becker:** Writing – review & editing, Investigation. **Michael Kokkoris:** Writing – review & editing, Methodology, Investigation, Conceptualization. **Matej Mayer:** Writing – review & editing, Investigation, Resources. **Georgios Provatas:** Writing – review & editing, Investigation. **Detlef Rogalla:** Writing – review & editing, Investigation. **Thomas Schwarz-Selinger:** Writing – review & editing, Resources.

Declaration of competing interest

The authors declare that they have no known competing financial interests or personal relationships that could have appeared to influence the work reported in this paper.

Acknowledgements

This work was fully supported by the Deutsche Forschungsgemeinschaft DFG under the project FO 1383/2-1. This work was also part of the IAEA-CRP F11023 under the Research Agreement 27046. We would also like to thank the staff of the RUBION facility of the Ruhr University Bochum and especially Mr. Roger Genschur for his support during the measurements.

Appendix

Table 1
Statistical and systematic errors contributing to the total estimated uncertainty.

Source of Uncertainty	(%)
N_{Au}/N_D	1.9
Target inhomogeneity	2.3
D-loss correction factor	< 1.0
Peak integration (Au_{el})	< 0.6
Peak integration (^{3}He(d,$p_0)^4$He)	2.0 – 4.6
Total estimated uncertainty	3.7 – 5.5

Table 2
Differential cross sections of the $^{2}H(^{3}He, p_0)^{4}He$ reaction. The reported errors correspond to the total estimated uncertainty.

E_{lab}(keV)	dσ/dΩ (mb/sr)					
	120°	130°	140°	150°	160°	170°
278 ± 2	12.7 ± 0.6	14.3 ± 0.7	14.8 ± 0.7	13.3 ± 0.6	14.8 ± 0.7	13.7 ± 0.6
327 ± 2	23.4 ± 1.2	23.3 ± 1.2	22.8 ± 1.1	21.7 ± 1.2	22.3 ± 1.2	21.5 ± 1.1
398 ± 2	33.5 ± 1.7	31.9 ± 1.6	29.1 ± 1.5	30.9 ± 1.6	32.7 ± 1.7	30.6 ± 1.5
426 ± 2	43.5 ± 2.0	42.7 ± 2.0	41.6 ± 1.9	40.5 ± 1.9	40.2 ± 1.9	39.8 ± 1.8
476 ± 2	51.0 ± 2.1	53.0 ± 2.1	50.0 ± 2.0	49.8 ± 2.0	50.0 ± 2.0	47.0 ± 1.9
526 ± 2	57.7 ± 2.4	55.0 ± 2.3	55.5 ± 2.3	55.1 ± 2.3	54.8 ± 2.3	52.6 ± 2.2
556 ± 2	61.4 ± 2.5	62.7 ± 2.6	58.8 ± 2.4	59.9 ± 2.5	58.9 ± 2.4	58.4 ± 2.4
586 ± 2	63.0 ± 2.7	61.6 ± 2.7	62.2 ± 2.7	63.0 ± 2.7	58.5 ± 2.6	62.0 ± 2.7
616 ± 2	66.1 ± 2.6	67.3 ± 2.7	64.9 ± 2.6	63.3 ± 2.5	64.3 ± 2.6	61.8 ± 2.4
646 ± 2	63.4 ± 2.7	65.5 ± 2.8	63.8 ± 2.7	61.9 ± 2.7	60.0 ± 2.6	61.3 ± 2.6
676 ± 2	62.9 ± 2.6	61.0 ± 2.5	60.8 ± 2.5	61.6 ± 2.6	61.3 ± 2.6	59.8 ± 2.5
706 ± 2	61.3 ± 2.6	62.4 ± 2.6	62.3 ± 2.6	58.5 ± 2.5	59.1 ± 2.5	58.1 ± 2.4
736 ± 2	60.0 ± 2.4	60.0 ± 2.5	57.5 ± 2.4	57.2 ± 2.4	55.5 ± 2.3	57.1 ± 2.3
776 ± 2	54.2 ± 2.3	51.2 ± 2.3	54.4 ± 2.4	50.7 ± 2.3	53.9 ± 2.4	51.2 ± 2.2
826 ± 2	51.3 ± 2.2	51.9 ± 2.2	51.5 ± 2.2	47.1 ± 2.1	46.7 ± 2.0	48.0 ± 2.0
876 ± 2	48.5 ± 2.0	47.1 ± 2.0	44.9 ± 1.9	44.5 ± 1.9	44.5 ± 1.9	44.5 ± 1.9
926 ± 2	43.1 ± 1.8	44.1 ± 1.8	42.8 ± 1.8	40.9 ± 1.8	39.4 ± 1.7	41.0 ± 1.7
977 ± 2	39.0 ± 1.6	39.2 ± 1.6	38.4 ± 1.6	36.2 ± 1.5	37.4 ± 1.6	38.4 ± 1.6
1027 ± 2	36.1 ± 1.6	34.8 ± 1.5	36.4 ± 1.6	34.6 ± 1.5	35.2 ± 1.5	34.8 ± 1.5
1077 ± 2	33.3 ± 1.4	32.6 ± 1.4	29.8 ± 1.3	28.8 ± 1.3	30.4 ± 1.3	29.4 ± 1.3
1127 ± 2	31.5 ± 1.2	29.8 ± 1.2	30.5 ± 1.2	29.7 ± 1.2	29.4 ± 1.2	28.6 ± 1.1
1177 ± 2	29.8 ± 1.2	27.7 ± 1.2	28.0 ± 1.2	28.1 ± 1.2	26.5 ± 1.2	26.5 ± 1.1
1226 ± 2	28.1 ± 1.2	25.0 ± 1.1	26.0 ± 1.1	24.7 ± 1.1	25.2 ± 1.1	24.4 ± 1.0
1277 ± 2	25.9 ± 1.1	27.4 ± 1.1	24.0 ± 1.0	24.9 ± 1.1	22.4 ± 1.0	22.7 ± 1.0
1327 ± 2	23.6 ± 1.0	22.8 ± 1.0	23.0 ± 1.0	22.5 ± 1.0	22.2 ± 1.0	21.0 ± 0.9
1377 ± 2	21.7 ± 0.9	20.6 ± 0.9	19.9 ± 0.9	19.5 ± 0.9	20.8 ± 0.9	19.1 ± 0.8
1427 ± 2	21.9 ± 0.9	20.9 ± 0.9	19.5 ± 0.8	20.4 ± 0.9	20.5 ± 0.9	20.0 ± 0.8
1477 ± 2	20.2 ± 0.9	20.2 ± 0.9	18.7 ± 0.8	18.8 ± 0.8	17.6 ± 0.8	17.6 ± 0.8
1527 ± 2	18.6 ± 0.8	17.3 ± 0.8	18.5 ± 0.8	17.1 ± 0.8	17.0 ± 0.8	16.9 ± 0.8
1577 ± 2	18.8 ± 0.8	17.5 ± 0.7	17.1 ± 0.7	17.4 ± 0.7	17.6 ± 0.7	16.2 ± 0.7
1627 ± 2	17.8 ± 0.7	16.3 ± 0.7	16.8 ± 0.7	16.9 ± 0.7	16.0 ± 0.7	15.9 ± 0.7
1677 ± 2	16.1 ± 0.7	16.4 ± 0.7	15.7 ± 0.7	14.7 ± 0.7	14.7 ± 0.7	14.9 ± 0.7
1727 ± 2	15.6 ± 0.7	14.6 ± 0.6	14.2 ± 0.6	13.6 ± 0.6	13.6 ± 0.6	14.7 ± 0.6
1777 ± 2	15.3 ± 0.7	15.4 ± 0.7	14.2 ± 0.6	14.3 ± 0.6	13.5 ± 0.6	13.7 ± 0.6
1827 ± 2	14.0 ± 0.6	15.4 ± 0.7	14.7 ± 0.6	14.1 ± 0.6	13.5 ± 0.6	13.0 ± 0.6
1876 ± 2	13.3 ± 0.6	13.3 ± 0.6	13.3 ± 0.6	12.5 ± 0.5	12.3 ± 0.5	12.1 ± 0.5
1926 ± 2	13.9 ± 0.6	13.2 ± 0.6	12.8 ± 0.6	13.4 ± 0.6	12.5 ± 0.6	12.4 ± 0.5
1976 ± 2	12.9 ± 0.5	11.9 ± 0.5	10.5 ± 0.5	11.5 ± 0.5	11.3 ± 0.5	11.2 ± 0.5
2076 ± 2	12.6 ± 0.6	12.0 ± 0.5	10.8 ± 0.5	12.1 ± 0.6	11.1 ± 0.5	10.9 ± 0.5
2176 ± 2	12.2 ± 0.5	11.0 ± 0.5	10.4 ± 0.5	10.1 ± 0.5	10.8 ± 0.5	10.3 ± 0.5
2275 ± 2	10.6 ± 0.5	10.4 ± 0.5	10.5 ± 0.5	9.7 ± 0.4	10.0 ± 0.5	9.8 ± 0.4
2375 ± 2	10.4 ± 0.5	10.5 ± 0.5	10.5 ± 0.5	9.2 ± 0.4	9.6 ± 0.5	9.7 ± 0.4
2475 ± 2	9.5 ± 0.4	9.3 ± 0.4	8.9 ± 0.4	8.6 ± 0.4	8.8 ± 0.4	9.2 ± 0.4
2574 ± 2	9.0 ± 0.3	9.1 ± 0.3	8.8 ± 0.3	8.8 ± 0.3	9.0 ± 0.3	8.4 ± 0.3
2674 ± 2	9.6 ± 0.5	8.7 ± 0.5	8.0 ± 0.4	7.9 ± 0.4	8.2 ± 0.4	8.8 ± 0.4
2774 ± 2	7.9 ± 0.4	8.7 ± 0.4	7.9 ± 0.4	7.8 ± 0.4	7.6 ± 0.4	7.9 ± 0.4
2874 ± 2	8.0 ± 0.4	7.8 ± 0.4	7.2 ± 0.4	8.0 ± 0.4	6.9 ± 0.4	7.6 ± 0.4
2973 ± 2	8.4 ± 0.4	7.9 ± 0.4	7.5 ± 0.4	7.6 ± 0.4	7.5 ± 0.4	8.3 ± 0.4
3073 ± 2	8.0 ± 0.4	8.0 ± 0.4	7.3 ± 0.4	8.2 ± 0.4	8.0 ± 0.4	7.7 ± 0.4
3173 ± 2	7.6 ± 0.4	7.2 ± 0.4	7.2 ± 0.4	7.2 ± 0.4	7.3 ± 0.4	7.2 ± 0.4
3272 ± 2	7.0 ± 0.4	7.1 ± 0.4	6.9 ± 0.4	6.6 ± 0.3	7.1 ± 0.4	7.2 ± 0.4
3372 ± 2	6.8 ± 0.3	6.8 ± 0.3	6.1 ± 0.3	6.5 ± 0.3	6.3 ± 0.3	6.6 ± 0.3
3472 ± 2	7.2 ± 0.4	6.6 ± 0.3	6.3 ± 0.3	6.6 ± 0.3	6.4 ± 0.3	6.7 ± 0.3
3571 ± 2	6.5 ± 0.3	5.9 ± 0.3	6.3 ± 0.3	6.9 ± 0.4	7.0 ± 0.4	6.9 ± 0.3
3671 ± 2	6.7 ± 0.3	6.5 ± 0.3	6.0 ± 0.3	6.3 ± 0.3	6.9 ± 0.3	6.8 ± 0.3
3770 ± 2	6.9 ± 0.3	6.5 ± 0.3	6.2 ± 0.3	6.00 ± 0.29	6.0 ± 0.3	6.5 ± 0.3
3870 ± 2	6.2 ± 0.3	6.0 ± 0.3	6.3 ± 0.3	5.9 ± 0.3	6.5 ± 0.3	6.8 ± 0.3
3970 ± 2	6.0 ± 0.3	5.9 ± 0.3	5.71 ± 0.29	6.4 ± 0.3	6.2 ± 0.3	6.8 ± 0.3

Data availability

All data will be available at the IBANDL website (https://www-nds.iaea.org/exfor/ibandl.htm).

References

[1] S. Brezinsek, Plasma-surface interaction in the Be/W environment: Conclusions drawn from the JET-ILW for ITER, *J. Nucl. Mater.* 463 (2015) 11–21, https://doi.org/10.1016/j.jnucmat.2014.12.007.

[2] M. Mayer, et al., Ion beam analysis of fusion plasma-facing materials and components: facilities and research challenges, *Nucl. Fusion* 60 (2) (Sep. 2020) 25001, https://doi.org/10.1088/1741-4326/ab5817.

[3] M. Mayer, E. Gauthier, K. Sugiyama, U. von Toussaint, Quantitative depth profiling of deuterium up to very large depths, *Nucl Instrum Methods Phys Res B* 267 (3) (2009) 506–512, https://doi.org/10.1016/j.nimb.2008.11.033.

[4] V.K. Alimov, M. Mayer, J. Roth, Differential cross-section of the D(3He,p)4He nuclear reaction and depth profiling of deuterium up to large depths, *Nucl Instrum Methods Phys Res B* 234 (3) (2005) 169–175, https://doi.org/10.1016/j.nimb.2005.01.009.

[5] B. Wielunska, M. Mayer, T. Schwarz-Selinger, U. von Toussaint, J. Bauer, Cross section data for the D(3He,p)4He nuclear reaction from 0.25 to 6MeV, *Nucl Instrum*

Methods Phys Res B 371 (2016) 41–45, https://doi.org/10.1016/j.nimb.2015.09.049.
[6] J.P. Zhu, X. Xiao, S. Yan, Y. Gao, J.M. Xue, Y.G. Wang, Measurement of differential cross section of D(3He,p)4He from 0.8MeV to 3.6MeV, *Nucl Instrum Methods Phys Res B* 412 (2017) 81–85, https://doi.org/10.1016/j.nimb.2017.07.020.
[7] M. Nocente, G. Gorini, J. Källne, M. Tardocchi, Cross section of the d + 3He → α + p reaction of relevance for fusion plasma applications, *Nucl. Fusion* 50 (5) (Apr. 2010) 55001, https://doi.org/10.1088/0029-5515/50/5/055001.
[8] W. Möller, F. Besenbacher, A note on the 3He + D nuclear-reaction cross section, *Nucl. Inst. Methods* 168 (1) (1980) 111–114, https://doi.org/10.1016/0029-554X(80)91239-2.
[9] T.W. Bonner, J.P. Conner, A.B. Lillie, Cross Section and Angular Distribution of the 3He(d,p)4He Nuclear Reaction, *Phys. Rev.* 88 (3) (Nov. 1952) 473–476, https://doi.org/10.1103/PhysRev.88.473.
[10] J.L. Yarnell, R.H. Lovberg, W.R. Stratton, Angular Distribution of the Reaction 3He (d, p)4He between 240 kev and 3.56 Mev, *Phys. Rev.* 90 (2) (Apr. 1953) 292–297, https://doi.org/10.1103/PhysRev.90.292.
[11] V. Foteinou, et al., Differential cross-section measurements for the 9Be(3He,3He0) 9Be elastic scattering and the 9Be(3He,px)11B reactions, *Nucl Instrum Methods Phys Res B* 542 (2023) 158–175, https://doi.org/10.1016/j.nimb.2023.06.016.
[12] D. Gockel, Kalibration der Ionenstrahlenergie des 4MV-Tandembeschleunigers am RUBION, Ruhr University Bochum, 2021. Master thesis.
[13] L. Hess, M. Mayer, T. Schwarz-Selinger, Cross-section data for the reactions 12C (3He,p0)14N to 12C(3He,p6)14N at energies up to 6 MeV, *Nucl Instrum Methods Phys Res B* 547 (Sep. 2024) 165141, https://doi.org/10.1016/j.nimb.2023.165141.
[14] M. Mayer, "SimNRA User's Guide: Version 7.03.".
[15] J.F. Ziegler, M.D. Ziegler, J.P. Biersack, SRIM – The stopping and range of ions in matter (2010), *Nucl Instrum Methods Phys Res B* 268 (11) (2010) 1818–1823, https://doi.org/10.1016/j.nimb.2010.02.091.
[16] T. J. *et al.*, "Program Tv," 2007, *Institute for Nuclear Physics, Cologne* .
[17] T. Schwarz-Selinger, A. von Keudell, W. Jacob, Plasma chemical vapor deposition of hydrocarbon films: The influence of hydrocarbon source gas on the film properties, *J Appl Phys* 86 (7) (Oct. 1999) 3988–3996, https://doi.org/10.1063/1.371318.
[18] Q. Yang, D.J. O'Connor, Z. Wang, Empirical formulae for energy loss straggling of ions in matter, *Nucl Instrum Methods Phys Res B* 61 (2) (1991) 149–155, https://doi.org/10.1016/0168-583X(91)95454-L.
[19] A.F. Gurbich, SigmaCalc recent development and present status of the evaluated cross-sections for IBA, *Nucl Instrum Methods Phys Res B* 371 (2016) 27–32, https://doi.org/10.1016/j.nimb.2015.09.035.
[20] "Guide to the Expression of Uncertainty in Measurement," 1995, *International Organization for Standardization*.
[21] H.-S. Bosch, G.M. Hale, Improved formulas for fusion cross-sections and thermal reactivities, *Nucl. Fusion* 33 (12) (Dec. 1993) 1919, https://doi.org/10.1088/0029-5515/33/12/513.